Physica Scripta. Vol. T68, 17–20, 1996

Nanofabricated Three Dimensional Photonic Crystals Operating at Optical Wavelengths

C. C. Cheng,[1] V. Arbet-Engels,[2] A. Scherer[1] and E. Yablonovitch[2]

[1] Electrical Engineering Department, California Institute of Technology, Pasadena, CA 91125, U.S.A.
[2] Electrical Engineering Department, University of California, Los Angeles, Los Angeles, CA 90095-1594, U.S.A.

Received June 5, 1996

Abstract

We describe the nanofabrication of the first three-dimensional (3-d) photonic crystals with a forbidden photonic bandgap lying in the near infrared region of the electromagnetic spectrum, $1.1\,\mu m < \lambda < 1.5\,\mu m$, just beyond the electronic band-edge of GaAs. We fabricated these structures by chemically assisted ion beam etching through a triangular hole array mask, defined by electron beam lithography on GaAs. The 3-d forbidden photonic bandgap was spectrally tuned by 2-d lithographic control of the 3-d spatial periodicity. Optical transmission spectra were generally in good agreement with microwave frequency transmission on centimeter scale models. Nevertheless, we find that the mid-gap optical reflectivity is surprisingly sensitive to structural errors in the photonic crystal, degrading the optical rejection from an expected 95% to an observed 80%. We suggest that mid-gap attenuation in the most vulnerable k-space directions, rather than overall thickness, is the relevant Figure-of-Merit for nano-scale photonic crystals.

As electronics evolves towards opto-electronics, it is somewhat natural for researchers to devise artificial photonic crystal structures which behave toward electromagnetic waves in the same manner as natural semiconductor crystals behave toward Schrodinger waves. The possibility of a complete 3-d photonic bandgap has stimulated the imagination and led to a field [1, 2] of electromagnetic band structure engineering. Based on the similarities between the Schrödinger equation and Maxwell's equation, the terminology used to describe photon waves [3, 4] has been largely borrowed from solid state physics [5]: reciprocal lattice, Brillouin zones, dispersion relations, etc.

In a 3-d photonic bandgap, electromagnetic modes, spontaneous emission and zero point fluctuations are all absent. The insertion of a local defect in a photonic crystal leads to a high-Q, single-mode 3-d nano-cavity [6]. These nanocavities will ultimately permit full 3-d confinement in the tiniest optical mode volume $\approx (\lambda/2n)^3$, where n is the refractive index. The ability to control electromagnetic mode density has suggested the use of these artificial structures for applications in quantum optics such as photon number state squeezing [7], single mode light emitting diodes [8] and photon localization [4], the analog of Anderson localization [9] for electrons in disordered media.

In this paper we report the first nanofabricated 3-d photonic crystals operating at near-infrared wavelengths. Various crystal lattices with different Wigner–Seitz [10–13] real space unit cells have been investigated as possible photonic crystal structures. It is now recognized that diamond topology [14] or connectivity, within the fcc lattice [15], is the most favorable geometry for 3-d photonic bandgaps. We are concentrating on the triple hole structure, illustrated in Fig. 1, which relies upon 2-d electron beam lithographic patterning, where the third dimension of periodicity, is indirectly created by the criss-cross of adjacent, angle-etched, cylinders below the surface.

Our two key nanofabrication technologies [16] are high resolution electron beam lithography and anisotropic chemically assisted ion beam etching (CAIBE). Since the resolution [17] for the nanolithography process is significantly improved by decreased resist thickness, we expose 70 nm thick polymethyl-methacrylate (PMMA) to electron beam-writing. This lithographic working surface becomes the $\langle 111 \rangle$ plane of the photonic lattice. We develop out the triangular hole pattern in the exposed regions of PMMA in a 3 : 7 solution of Cellusolve : methanol, and use this perforated electron beam resist mask to define holes in a thin Au/Cr etch mask by ion milling. We find that a 100 nm Au/Cr layer provides sufficient etch rate selectivity in C_2F_6 reactive ion etching plasmas, to transfer our high resolution mask into 200 nm SiO_2. This layer, in turn can be used as an adequate ion milling mask to transfer the SiO_2 features into a more CAIBE-resistant 150 nm thick Nickel mask layer. The patterned Ni layer is then used during the anisotropic CAIBE etch to define the photonic crystal. For optical measurements, residual Nickel on the surface of the sample would be undesirable, thus we generally include a thin SiO_2 layer underneath the Nickel mask. We then angle etch by CAIBE until the Nickel mask is completely consumed, and complete the etching process with the mask consisting of optically transparent SiO_2. The sequence of progressively more durable masking layers is typically: PMMA/Au/Cr/SiO_2/Ni/SiO_2 on GaAs!

The sample is then mounted on a triangular holder which can be rotated by 120° and tilted off normal by 35.28° within the vacuum system, the operations required by Fig. 1. We sequentially etch the three angled holes through the Ni/SiO_2 mask by CAIBE using 1500 eV Ar^+ ions, assisted by Cl_2 reactive gas.

A possible Figure-of-Merit of these photonic crystals is the aspect ratio or depth-to-diameter ratio of the engraved cylinders. That in turn determines the number of the $\langle 111 \rangle$ lattice layers ($a/\sqrt{3}$ thick where a is the unit cube length) which consequently determines the functional performance of the crystal as parametrized for instance by mid-gap attenuation. The choice of complex masking layers is motivated by the required high etch rate selectivity relative to

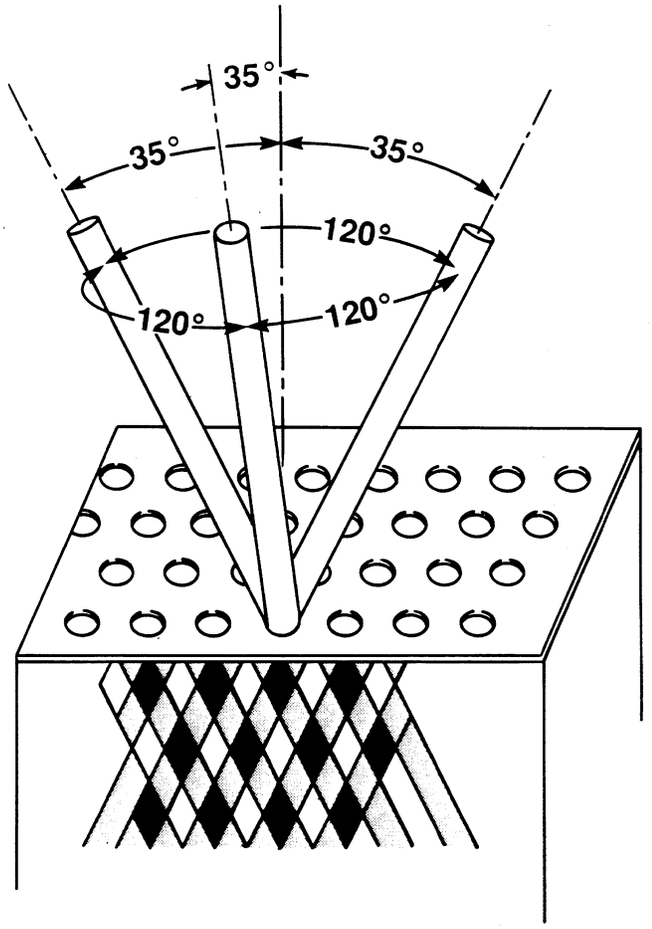

Fig. 1. A slab of dielectric material is covered by a mask consisting of a hexagonal array of holes. Each hole is drilled through three times at an angle of 35.26° away from the normal, and spread out 120° on the azimuth, corresponding to the ⟨110⟩, ⟨101⟩ and ⟨011⟩ directions of the fcc lattice, respectively. The mask surface defines a ⟨111⟩ photonic crystal plane.

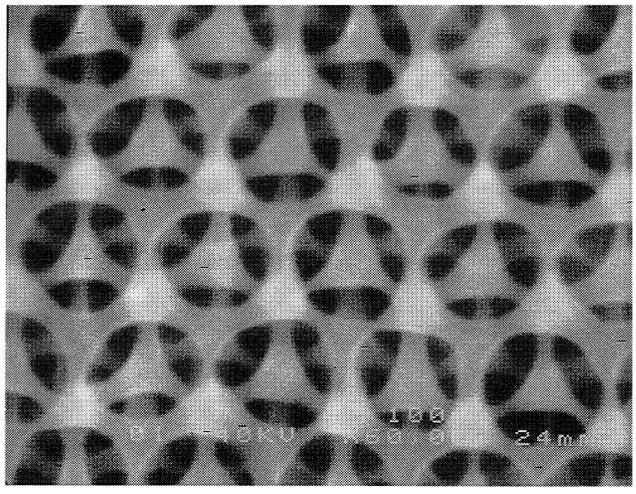

(a)

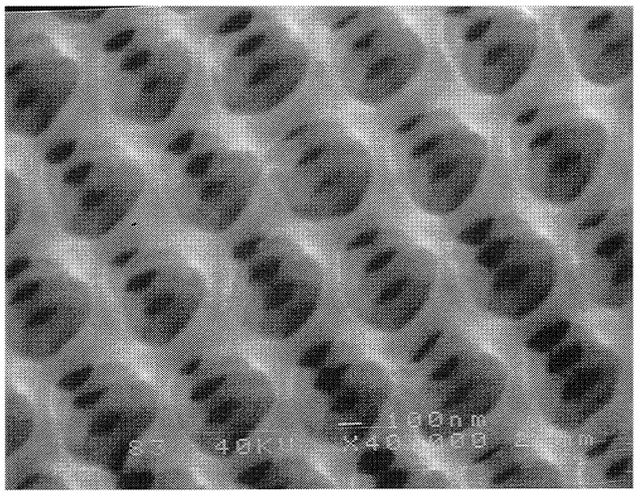

(b)

Fig. 2. (a) Normal incidence SEM micrograph of a photonic crystal revealing multiple layers in the structure, with a center-to-center spacing $a/\sqrt{2} = 460\,\text{nm}$. (b) SEM picture of a photonic crystal tilted 25° off-normal showing roughly 3 successive layers of horizontal ribs carved into the GaAs.

the GaAs substrate. Erosion of the sidewalls at the top of the photonic crystal, while the bottom of the structure is being etched, weakens the electromagnetic spatial coherence and destructive interference upon which the photonic bandgap depends. Exacerbating the problem, thin masks are necessary in order to minimize lateral shadowing of the unmasked semiconductor surface during the angle etch, which could distort the original circular pattern. The observed selectivity during our anisotropic CAIBE process was in excess of 30 : 1, allowing a usable aspect ratio of roughly 10 : 1.

Figure 2(a) depicts a top view scanning electron micrograph (SEM) of the ⟨111⟩ lattice plane of our photonic crystal. The hexagonal array of holes in the GaAs replicates the mask shown in Fig. 1, having a center-to-center spacing of $\approx 460\,\text{nm}$ ($a/\sqrt{2}$). With a hole diameter of $\approx 330\,\text{nm}$, the ribs remaining behind are $< 130\,\text{nm}$ thick, demanding precision lithography. These length scales are much finer than would be suggested by the vacuum wavelength, owing to the high refractive index of GaAs. Small deviations in geometrical dimensions of the structure can result in significant spectral shifts of the photonic gap, as will be illustrated in Fig. 4. Hence, at these length scales, a tremendous demand is placed on the precision of the electron-beam writing and pattern transfer technologies. Figure 2(b) is an SEM picture with the sample tilted 25° away from the ⟨111⟩ axis. We can observe at least three successive vertical layers carved into GaAs, each layer being $a/\sqrt{3}$ thick corresponding to an overall photonic crystal thickness of $\approx 1.5\,\mu\text{m}$.

The optical transmission characteristics of the nanofabricated photonic crystals were measured through a $40 \times 40\,\mu\text{m}^2$ aperture in a Nickel mask, at room temperature, with light directed along the photonic ⟨111⟩ axis parallel to the L_3 point in the photonic reciprocal space [15] (surface normal to the GaAs wafer). The Ni aperture mask was thick enough to insure total opacity outside the area of the photonic crystal. A quartz tungsten halogen lamp along with an $f/4$ monochromator delivered wavelengths between 0.9 μm and 1.7 μm, within the transparent region of GaAs. This light was then focused onto the sample using a off-axis paraboloid mirror. Reflective optical elements were necessary to eliminate chromatic aberration, a severe problem with refractive optics over the wide spectral range required. The transmitted light was then collected in an InGaAs photodetector. For absolute transmission calibration, the optical spectrum was normalized to the spectrum of an adjacent unpatterned $40 \times 40\,\mu\text{m}^2$ aperture.

Measured optical transmission spectrum of a GaAs photonic crystal is shown by the solid line in Fig. 3. The photonic bandgap lies in the near infrared with a width of about

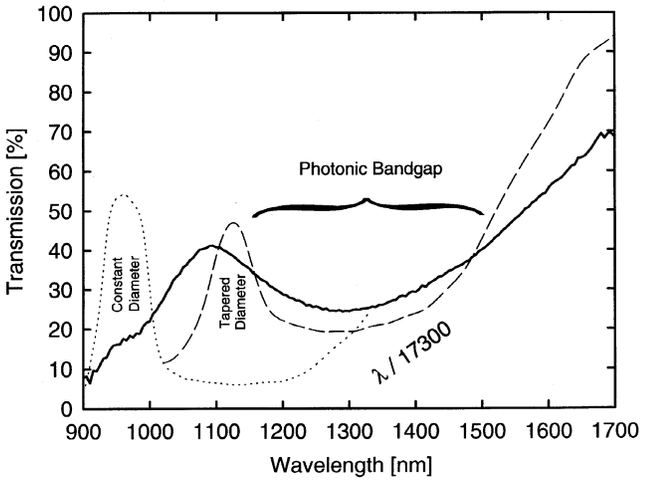

Fig. 3. Measured transmission spectra of a nanofabricated photonic crystal (solid line) and the corresponding microwave scale models (dotted and dashed lines). The microwave models were fabricated out of Stycast (refractive index matching that of GaAs), using conventional machine tools. Microwave-lengths were divided by a 17300 scaling factor to fit on the same graph as the near-infrared photonic crystal. The "Constant Diameter" spectrum corresponds to a scale model with fixed hole diameter. The "Tapered Diameter" curve represents a transmission spectrum through a microwave structure with a 12% taper as we penetrate vertically into the lattice structure. Curve fitting suggests that the nano-scale photonic crystal has a taper somewhat less than 12%, accompanied by some inhomogeneous broadening.

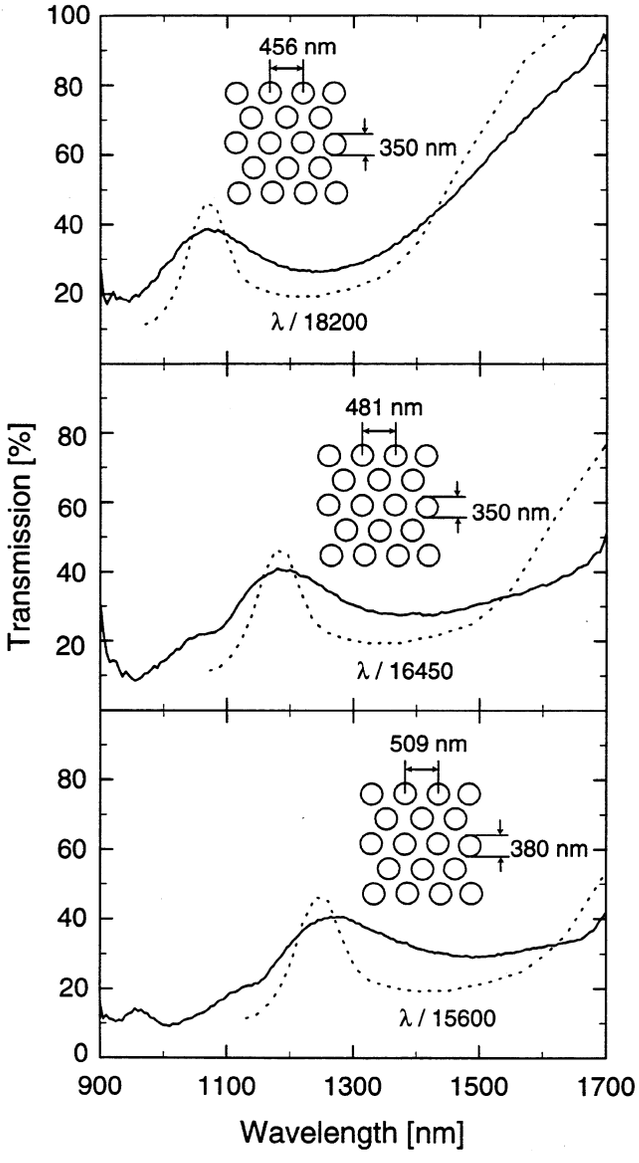

Fig. 4. Transmission spectra of nanofabricated photonic crystals showing tunability of the bandgap features with varying hole spacings and sizes. The actual dimensions were recorded from SEM micrographs. The dotted lines are the corresponding scaled transmission spectra of the "Tapered Diameter" scale model.

19% of its mid-gap frequency. We notice that while the transmission at the photonic valence band edge approaches unity, the photonic conduction band exhibits only ≈40% transmission. This is quite common [18] in photonic crystals, and is due the electromagnetic mode mismatch between external plane waves and internal Bloch conduction band modes. The dotted and dashed lines on Fig. 3 labeled "Constant Diameter" and "Tapered Diameter" correspond to microwave transmission spectra for 17300× scale models made of Stycast with a dielectric constant = 12 matching the dielectric constant of GaAs. The scale models were fabricated using precision tools in a conventional machine shop, and consisted of 2.5 lattice layers, ($2.5 \times a/\sqrt{3}$), bonded to a thick slab of Stycast material meant to simulate the GaAs substrate.

In order to represent the optical and microwave spectra on the same graph, the microwave-lengths were divided by the scaling factor, 17300, for the photonic crystal of Fig. 3. The evaluation of this factor deserves special clarification. At first glance, the GaAs photonic crystal is a compressed version of the "Constant Diameter" microwave model with the dielectric constant scaling relation $\varepsilon_{\mu\text{-wave}}(r) = \varepsilon_{\text{optical}}(r/s)$, where "$s$" is the ratio of center-to-center spacing between the two structures. However, the microwave model was fabricated using conventional drill bits with a round cross-section, while the GaAs photonic crystal was angle etched through a circular hole pattern, producing elliptical cross-section cylinders. The eccentricity of the cylinders is given by cos 35.26° = 0.82. This results in a larger remaining volume fraction of dielectric material in the GaAs photonic crystal, and consequently a red-shift in the forbidden gap relative to the round hole case. The actual shift was determined using the oval hole calculations by Qian *et al.* [19], with infrared refractive index taken from the literature [20].

"Tapered Diameter" and "Constant Diameter" are meant to distinguish microwave models with and without a taper in the drilled hole diameter, dashed and dotted lines respectively on Fig. 3. The "Constant Diameter" microwave scale model attenuates electromagnetic radiation by 95% at mid-gap. The dashed line shown as "Tapered Diameter" represents a similar microwave model, identical at the top surface, but with tapered holes meant to simulate the expected decreased hole diameter in the GaAs photonic crystal as we ion etch into the material. The overall taper was approximately 4.8% per layer or 12% from top to bottom. By weakening the interference effects on which the photonic bandgap depends, the taper considerably degrades the mid-gap attenuation to 80%. Further, since less dielectric material is removed due to the decreasing hole diameter, the band-edges also happen to shift towards longer wavelengths. The mediocre spectral match between the GaAs photonic crystal and the tapered microwave scale model indicates that the structural precision of our current nanofabrication process is no better than 12%. Small variations

in hole diameter, as seen in Fig. 2, are most likely responsible for some inhomogeneous broadening. (Parenthetically, computational modeling of the tapered geometry is sufficiently challenging, that it leaves a role for scale model experimentation as done here.)

Further evidence for the accurate scaling between microwave and optical wavelengths is illustrated in Fig. 4, where we show a systematic wavelength shift in the conduction band peak as a function of hole diameters and spacings (recorded from SEM micrographs). The dotted lines are the corresponding transmission spectra of the tapered microwave model.

Thus far our best mid-gap attenuation for a GaAs nanofabricated photonic crystal has been 80%. This modest performance should be tempered by the observation that we are testing the photonic crystal in its most vulnerable k-space direction L_3 where the vertical periodicity is indirectly produced by the inter-section of holes below the surface. Contrariwise, the periodicity in the lateral directions is lithographically, coherently, written over the 40 μm aperture. Therefore the optical attenuation in the lateral directions is probably close to ideal, and does not represent a meaningful Figure-of Merit for photonic crystal nanostructures.

There are six lateral hexagonal facets to the Brillouin Zone, and two vertical hexagonal facets in our geometry. A weighted average of spontaneous emission in all directions would probably be inhibited by $\approx 95\%$, even though the inhibition in the vertical direction is only 80%.

For stimulated emission, the lasing mode with the highest reflectivity would naturally be sought out, depending on which cavity modes are designed in. The lateral reflectivity is probably more than sufficient to allow lasing in our photonic crystals. We believe that these photonic crystals are already of sufficient quality to allow commencement of experiments on both spontaneous and stimulated emission.

Acknowledgements

This work was supported by the National Science Foundation under grant number ECS-9310681, and the Army Research Office under grant number DAAH04-93-0227.

References

1. See for example the articles in the special issue of J. Opt. Soc. Am. **B10**, (February, 1993).
2. Joannopoulos, J. D., Meade, R. D. and Winn, J. N., "Photonic Crystals" (Princeton University Press, Princeton, NJ 1995).
3. Yablonovitch, E., Phys. Rev. Lett. **58**, 2059 (1987).
4. John, S., Phys. Rev. Lett. **58**, 2486 (1987).
5. Ashcroft, N. W. and Mermin, N. D., "Solid State Physics" (Saunders College Publishing, New York 1976).
6. Yablonovitch, E. *et al.*, Phys. Rev. Lett. **67**, 3380 (1991).
7. Yamamoto, Y., Machida, S. and Richardson, W. H., Science **225**, 1219 (1992).
8. Yablonovitch, E., J. Opt. Soc. Am. **B10**, 283 (1993).
9. Anderson, P. W., Phys. Rev. **109**, 1492 (1958).
10. Sozuer, H. S. and Haus, J. W., J. Opt. Soc. Am. **B10**, 296 (1993).
11. Hornreich, R. M., Shtrikman, S. and Sommers, C., Phys. Rev. **B49**, 10914 (1994).
12. Ozbay, E. *et al.*, Appl. Phys. Lett. **64**, 2059 (1994).
13. Fan, S., Villeneuve, P. R., Meade, R. D. and Joannopoulos, J. D., Appl. Phys. Lett. **65**, 1466, (1994).
14. Ho, K. M., Chan, C. T. and Soukoulis, C. M., Phys. Rev. Lett. **65**, 3152 (1990).
15. Yablonovitch, E., Gmitter, T. J. and Leung, K. M., Phys. Rev. Lett. **67**, 2295 (1991).
16. Cheng, C. C. and Scherer, A., J. Vac. Sci. Technol. **B13**(6), 2696 (1995).
17. Scherer, A., Jewell, J. L. and Harbison, J. P., Opt. Phot. News **2**, 9 (1991).
18. Robertson, W. M. *et al.*, Phys. Rev. Lett. **68**, 2023 (1992).
19. Qian, G. X. and Leung, K. M., Phys. Rev. **B44**, 11482 (1991).
20. "Properties of Gallium Arsenide" (INSPEC Publication, 1990), p. 157.